Vietnam Journal of Catalysis and Adsorption
Tạp chí xúc tác và hấp phụ Việt Nam

https://jca.edu.vn

Synthesis and application of spherical Alginate/$CaCl_2$ hydrogel beads for water harvesting from air

Tran Thi Khanh Linh[1,2], Nguyen Thi Huong[2,*], Vu Minh Thanh[2]

[1] *Vietnam Military Medical Academy, 160 Phung Hung, Ha Dong, Hanoi, Vietnam*
[2] *Institute of Materials, Biology and Environment, 17 Hoang Sam, Nghia Do, Hanoi, Vietnam*
** Email: nguyenhuong0916@gmail.com*

ARTICLE INFO

Received: 04/08/2025
Accepted: 07/09/2025
Published: 30/09/2025

Keywords:
Alginate; hydrogel;
Atmospheric water harvesting;
AWH

ABSTRACT

This study presents the synthesis and characterization of spherical hydrogel materials based on alginate cross-linked with Ca^{2+} cations, with particle diameters ranging from 0.20 to 0.25 cm. The structural properties of the synthesized materials were evaluated using X-ray diffraction, scanning electron microscopy (SEM), energy-dispersive X-ray mapping (EDX-mapping), Fourier-transform infrared spectroscopy (FT-IR), and Brunauer-Emmett-Teller (BET) surface area analysis. The water vapor adsorption capacity of the Alginate/$CaCl_2$ hydrogel spheres reached 220 – 270 wt% relative to the dry weight, depending on ambient humidity conditions, with equilibrium sorption capacity reaching 80% of the saturation value within 4 hours. Furthermore, the material demonstrated excellent regeneration capability at 140°C, maintaining 80-90% of its original sorption capacity after 3 cycles regeneration cycles. These results indicate the potential of alginate-based hydrogel spheres as efficient and recyclable sorbents for sustainable atmospheric water harvesting applications.

Introduction

Atmospheric water harvesting (AWH) has emerged as a promising technology for freshwater production, particularly valuable for remote, arid regions and for marine emergency applications [1]. Current AWH systems rely on various moisture-adsorbing materials, including metal-organic frameworks (MOFs), zeolites, and hygroscopic salt-containing hydrogels [2-4]. However, these materials often face limitations in terms of regeneration efficiency and cycling stability [1].

In this context, hydrogel materials have emerged as a superior solution. With their three-dimensional cross-linked polymer networks capable of holding vast amounts of water (up to 90% by weight), hydrogels possess unique properties such as swelling-deswelling, superabsorption, and responsiveness to external stimuli, gradually overcoming the drawbacks of durability and regenerability found in traditional materials [5,6]. Among them, alginate, a natural polysaccharide, is an ideal candidate. The structure of Alginate, composed of interconnected β-D-mannuronic (M) and α-L-guluronic (G) blocks, allows it to form cross-links with divalent or trivalent metal cations.

The gelation mechanism of alginate with calcium ions (Ca^{2+}) is of particular interest and is widely described by the "Egg-box model" [7]. According to this model, Ca^{2+} ions act as bridges, selectively binding to the guluronic-rich blocks (G-blocks) of different Alginate chains. This coordination creates a stable three-dimensional structure, imparting the material with both necessary mechanical strength and flexibility. The Ca^{2+} ions from the salt $CaCl_2$ are also potent hygroscopic agents themselves, promising a synergistic effect that both

https://doi.org/10.62239/jca.2025.041

enhances the system's water-absorbing capacity and stabilizes the hydrogel bead structure [8,9]. Theoretical studies have also indicated that factors such as the ionic radius and valence of the cations can influence the cross-linking density and the structure of the gel network [10,11]. More recently, molecular dynamics simulations have highlighted the importance of water-polymer interactions in determining the gel's properties [12].

Despite the recognized potential of the Alginate/$CaCl_2$ system, a systematic investigation into the effect of $CaCl_2$ concentration on the morphology, structure, and especially the water harvesting performance of the hydrogel beads remains limited. Therefore, this study focuses on the synthesis of spherical Alginate/$CaCl_2$ hydrogel beads with varying $CaCl_2$ contents. The properties and morphology will be characterized and their moisture sorption capabilities will also be evaluated under atmospheric conditions, aiming to identify the optimal formulation for atmospheric water harvesting applications.

Experimental

Materials

Sodium Alginate (alginic acid sodium salt from brown algae, Merck) and anhydrous calcium chloride (granular, Merck), which served as the Ca^{2+} ion source for hydrogel cross-linking, were used. Deionized (DI) water (TDS < 5) was used as a solvent and for washing. Filter paper (ø 110 mm) was purchased from Whatman Ltd. (UK). All chemicals were of analytical grade and used as received.

Methods

Synthesis of Alginate/$CaCl_2$ Hydrogel Beads

Sodium Alginate solutions were prepared by dissolving Alginate powder in DI water to achieve concentrations ranging from 1% to 5% (w/w), with dissolution assisted by an ultrasonic bath (Sonics & Materials - VCX500; 500 W, 20 kHz). The cross-linking solutions were prepared by dissolving $CaCl_2{\cdot}2H_2O$ in DI water to obtain concentrations ranging from 30 g/100 mL to 80 g/100 mL.

The hydrogel beads were formed by the dropwise addition of the Alginate solution (at a rate of 3 mL/min) into a petri dish containing 30 mL of the $CaCl_2$ solution. This process was conducted at room temperature (approx. 25 °C) with gentle agitation of the petri dish to ensure the formation of spherical beads and to prevent agglomeration. After gelation was complete, the hydrogel beads were collected by filtration and subsequently washed thoroughly with distilled water multiple times to remove excess $CaCl_2$ from the surface. Finally, the beads were dried at 140 °C for 24 hours. The resulting material consisted of light-brown, spherical beads with a diameter of approximately 0.20–0.25 cm, which were stored in sealed glass vials to protect them from moisture (Fig 1).

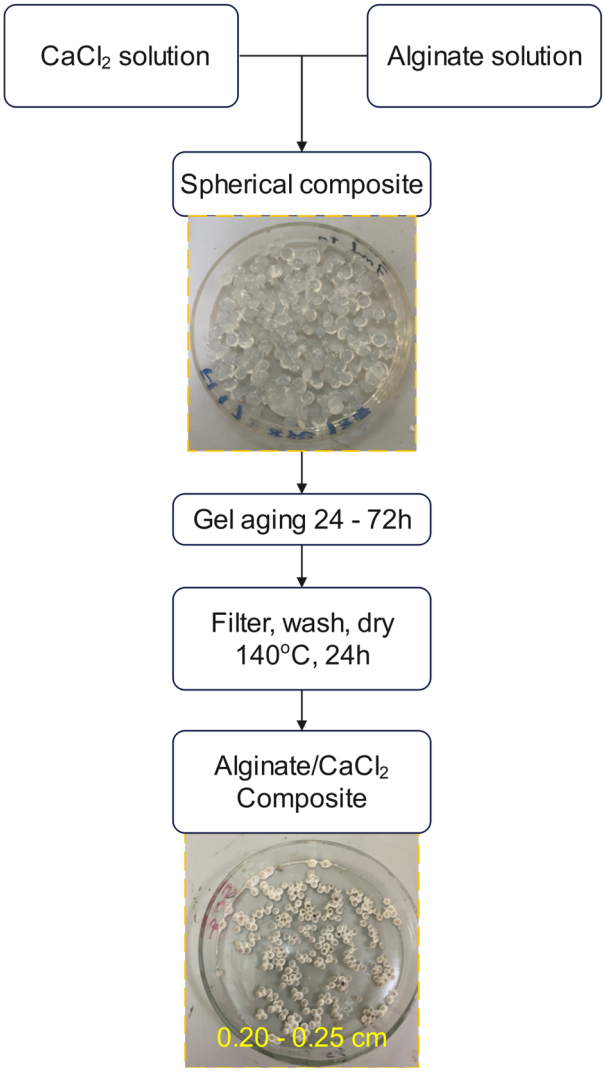

Fig 1: Synthesis scheme of the Alginate/$CaCl_2$ composite

Characterization Methods

The phase structure of the materials was identified using an X-ray diffractometer (XRD, AERIS, Netherlands). The molecular structure was investigated using a Fourier-Transform Infrared Spectrometer (FT-IR, Thermo Scientific - NICOLET iS50). Brunauer-Emmett-Teller (BET) analysis for surface area and porosity was conducted on a Tristar II 3030 plus instrument. The microstructure of the materials was observed using a scanning electron microscope (SEM, JEOL JSM-IT200) equipped with an energy-dispersive X-ray spectroscopy (EDS) system, operating under an accelerating voltage of 10 kV.

https://doi.org/10.62239/jca.2025.041

The water vapor adsorption capacity and reusability of the material were evaluated as follows: The dynamic equilibrium adsorption capacity of the Alginate/$CaCl_2$ composite was investigated at room temperature (25–27 °C) under two relative humidity (RH) conditions: 60% and 90%. After each adsorption cycle, the material was regenerated via thermal treatment at 140 °C for 8 hours. The process was repeated for three cycles to assess reusability.

Results and discussion

Optimization of Synthesis Parameters

Effect of Alginate Concentration on Material Morphology

The effect of Alginate concentration on the microstructure and morphology of the hydrogel beads was investigated using SEM (Fig 2). For this experiment, the $CaCl_2$ solution concentration was held constant at 60 g/100 mL, while the Alginate solution concentration was varied from 1% to 5% (w/w).

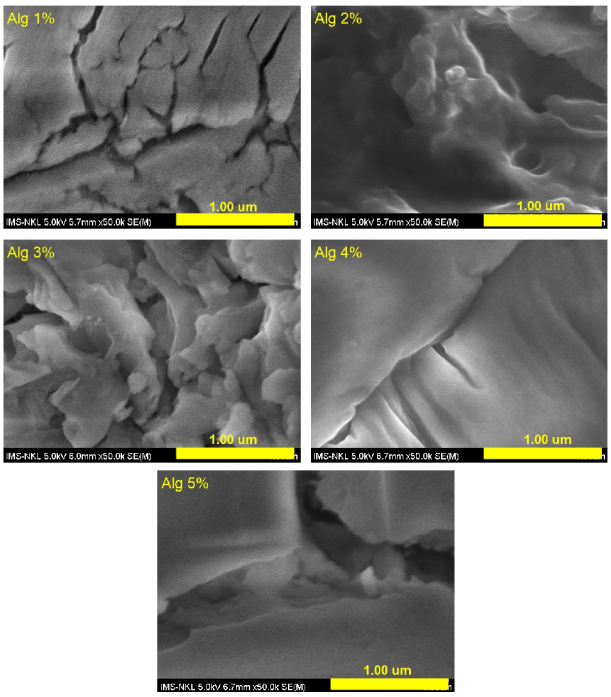

Fig 2: SEM images of Alginate/$CaCl_2$ composite

The results show that at a low Alginate concentration (1%), the material forms a film-like layer with random cracks and low porosity. As the Alginate concentration was increased to 2% and 3% the material's surface transformed significantly into a three-dimensional structure with numerous pores and cavities. This change is attributed to the higher concentration of carboxyl groups provided by the increased Alginate content, which enhances the cross-linking density between Ca^{2+} ions and the polymer chains, thereby forming a more porous network. Notably, the 3% Alginate sample exhibited a hierarchical structure with optimal porosity, featuring a system of large, interconnected pores, channels, and continuous grooves. This morphology is expected to increase the specific surface area and adsorption capacity of the material. However, upon further increasing the Alginate concentration to 4 % and 5% the porous structure collapsed, and the surface became denser with fewer pores. This is likely due to an excessively high cross-linking density, which renders the structure brittle and prone to collapse during the drying process.

Structural Characterization of Alginate/$CaCl_2$ composite

X-ray Diffraction (XRD) Analysis: The XRD pattern of the optimized sample (Fig 3) displays a broad, featureless halo at 2θ angles below 20°, which is characteristic of the amorphous nature of the Alginate polymer matrix. In contrast, a series of sharp diffraction peaks are observed in the 2θ range of 25° to 50°, with prominent peaks at 29.5°, 32.0°, 45.5°, and 56.5°. These peaks correspond to the crystalline planes of $CaCl_2$ [13]. During the complete dissolution of $CaCl_2$ in deionized (DI) water, Ca^{2+} ions undergo partial hydrolysis, which can lead to the formation of $Ca(OH)_2$ after heat treatment. This phenomenon can explain the appearance of weak, unusual peaks around 15°, 35°, 40°, and 50° in the XRD spectra. The high intensity and narrowness of the peaks indicate that the $CaCl_2$ exists in a highly crystalline form. This result confirms the successful formation of a composite system, where crystalline $CaCl_2$ is dispersed within an amorphous Alginate matrix.

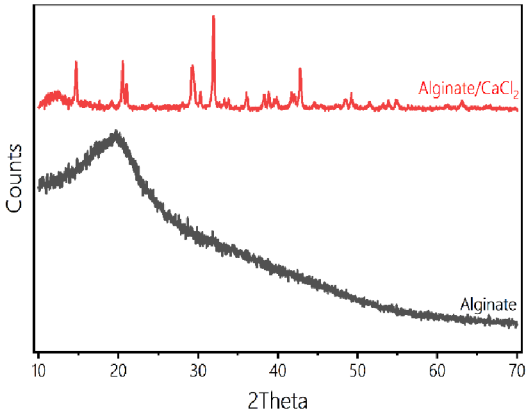

Fig 3: XRD pattern of Alginate and Alginate/$CaCl_2$ composite

Fourier-Transform Infrared (FT-IR) Spectroscopy Analysis: The FT-IR spectrum of the material (Fig 4a) exhibits characteristic absorption bands. A broad band in the 3400-3500 cm^{-1} region corresponds to the

https://doi.org/10.62239/jca.2025.041

vibrations of -OH groups (from Alginate and adsorbed water molecules). Notably, a peak at 1612 cm^{-1} is characteristic of the bending vibration of physically adsorbed water molecules, indicating the material's strong affinity for moisture, which is primarily due to the hygroscopic nature of $CaCl_2$. Furthermore, peaks in the 400-600 cm^{-1} region can be attributed to Ca-O bonds formed during the cross-linking process, confirming the interaction between calcium ions and the Alginate chains [14,15].

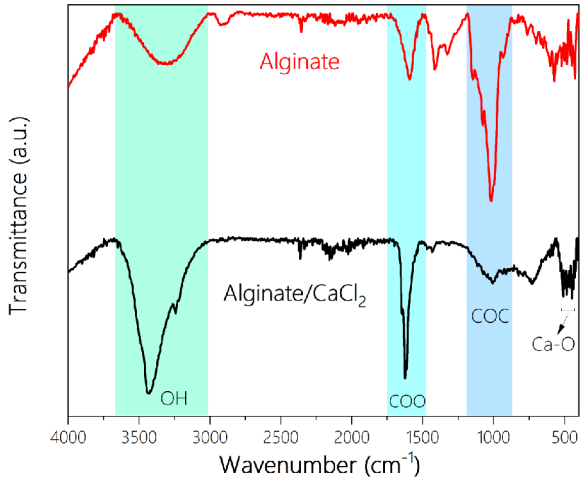

Fig 4: FTIR spectrum of Alginate and Alginate/$CaCl_2$ composite

Surface Area (BET) Analysis: The results from the N_2 adsorption-desorption isotherm showed that the specific surface area of the composite material, calculated using the BET method, is 12.9 m^2/g .

EDX-Mapping analysis: SEM-EDX elemental mapping (Fig 5a) revealed uniform distribution of oxygen (O Ka1) and calcium (Ca Ka1) across the hydrogel surface, confirming successful formation of calcium alginate networks through ionic crosslinking mechanisms [16]. The sparse distribution of carbon (C Ka1_2) and minimal presence of sodium (Na Ka1_2) and chlorine (Cl Ka1) indicated effective ion exchange during gelation, where Ca^{2+} ions replaced Na^+ ions in the alginate matrix [15]. The corresponding EDX spectrum (Figure 5b) demonstrated characteristic peaks for Cl (~2.6 keV) and Ca (~3.7 keV), with lower intensity signals for C, O, and Na, consistent with the chemical composition of calcium alginate hydrogels formed via the "egg-box" model crosslinking mechanism [17]. The Ca/Cl peak intensity ratio and elemental distribution patterns confirmed the structural integrity and homogeneous crosslinking density throughout the alginate/$CaCl_2$ hydrogel matrix, validating successful hydrogel formation through divalent cation coordination with guluronic acid blocks in the alginate backbone [18].

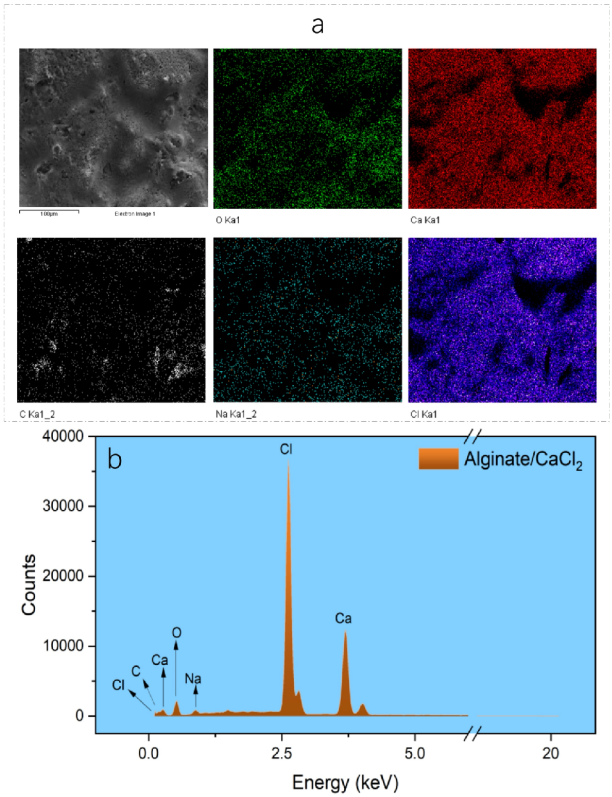

Fig 5: Mapping scan images (a) and EDX data (b) of Alginate/$CaCl_2$

Water Vapor Adsorption and Regeneration Performance

The water vapor adsorption capacity of the Alginate/$CaCl_2$ composite material was evaluated under dynamic conditions at two relative humidity (RH) levels: 70% and 90% (Fig 6).

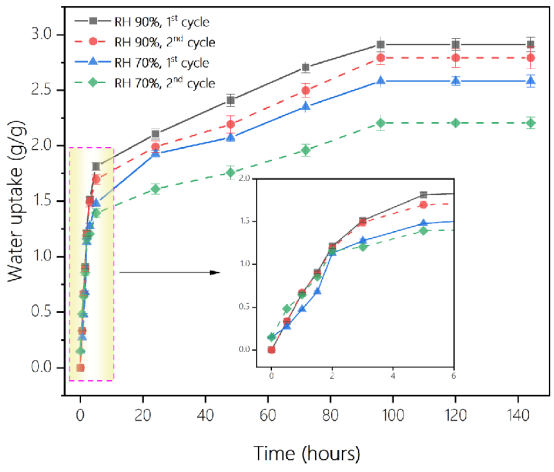

Fig 6: Water vapor adsorption kinetics of the Alginate/$CaCl_2$ composite at RH 70% and RH 90%, showing performance during the 1st cycle and after regeneration

The results indicate that the material's adsorption capacity is strongly dependent on the ambient humidity. At 90% RH, the material achieved an equilibrium

https://doi.org/10.62239/jca.2025.041

adsorption capacity of around 2.91 g/g, whereas at 70% RH, the capacity reached 2.58 g/g. Kinetically, the adsorption process was rapid in the initial phase, reaching over 80% of its maximum capacity within just 4–5 hours, and approached saturation after approximately 100 hours.

Table 1: Comparison the water uptake performance of various AWHs materials.

Type	Name	Water uptake (g/g)	Relative humidity (%)	Year
MOFs	MOF-808/ $CaCl_2/Fe_3O_4$	1.02	75	2023 [21]
	UiO-66-NH_2/C/ LiCl	2.4	90	2024 [22]
	PCGF-MMOF	0.36	90	2023 [23]
HICs and derivatives	MnO_2	1.8	80	2020 [24]
	LiCl,ACFF	3.6	90	2021 [25]
Hydrogel	NIPAM,CNT, $CaCl_2$	1.75	80	2018 [26]
	AAm,PPy, dopamine	1.54	90	2020 [27]
	AEtMA, acetate	1	85	2021 [28]
	Alginate/$CaCl_2$ hydrogel	2.91	90	This work
		2.58	70	

Similarly, the reusability of the material was investigated. After the first regeneration cycle via thermal treatment, a slight decrease in the material's adsorption capacity was observed. Specifically, the capacity decreased to 2.79 g/g (a 4.1% reduction) at 90% RH and to 2.20 g/g (a 14.7% reduction) at 70% RH. Although the time required to reach equilibrium did not change significantly, this loss in capacity can be attributed to minor alterations in the material's porous microstructure under thermal stress, or to a partial loss of Ca^{2+} ion cross-links during the sorption-desorption process [19,20]. As discussed, the experimental procedure was conducted with replicates to calculate the error and assess the accuracy of the data. An interesting observation was that the error increased after the material regeneration process at both humidity levels. In the 1st cycle, the error ranged from 1.5% to 2.5%, but in the 2nd cycle, the error increased to the range of 2.0% to 3.5%. This finding suggests that although the regeneration process achieved relatively high efficiency, it was not completely thorough. Nevertheless, when compared to other types of AWHs materials (shown in Table 1), the Alginate/$CaCl_2$ material demonstrates significant potential for practical applications in atmospheric water harvesting due to its high adsorption capacity under the same humidity conditions.

Conclusion

In this study, the spherical Alginate/$CaCl_2$ composite hydrogel was successfully developed and characterized for atmospheric water harvesting applications. The composite with 3% alginate concentration produced optimal hierarchical porous morphology, and the formation of crystalline $CaCl_2$ dispersed within an amorphous alginate matrix was confirmed through comprehensive XRD, FT-IR, and SEM-EDX analyses. The findings demonstrate that the composite achieves exceptional water vapor adsorption capacities of 2.91 g/g and 2.58 g/g at 90% and 70% relative humidity, respectively, with rapid kinetics reaching 80% saturation within 4–5 hours. The material's regeneration capability was also validated, maintaining good reusability with only 4.1 – 14.7% capacity reduction after thermal cycling, thereby establishing the viability of this bio-based composite for practical atmospheric water harvesting in water-scarce regions.

References

1. X. Zhou, H. Lu, F. Zhao, G. Yu, ACS Materials Letters 2 (2020) 671. https://doi.org/10.1021/acsmaterialslett.0c00130
2. Q. Ma, Q. He, P. Yin, H. Cheng, X. Cui, Q. Yun, H. Zhang, Advanced Materials 32 (2020) 2003720. https://doi.org/10.1002/adma.202003720
3. H.Z. Zhao, T. Liu, Z.Y. Wang, Q.W. Li, T.H. Wu, M. Zhang, International Journal of Environmental Science and Technology 18 (2021) 2693. https://doi.org/10.1007/s13762-020-02989-2
4. P.A. Kallenberger, M. Fröba, Communications Chemistry 1 (2018) 28. https://doi.org/10.1038/s42004-018-0028-9
5. A. Entezari, M. Ejeian, R. Wang, ACS Materials Letters 2 (2020) 471. https://doi.org/10.1021/acsmaterialslett.9b00315
6. D.K. Nandakumar, S.K. Ravi, Y. Zhang, N. Guo, C. Zhang, S.C. Tan, Energy & Environmental Science 11 (2018) 2179. https://doi.org/10.1039/C8EE00902C
7. V. Annisa, T.N.S. Sulaiman, A.K. Nugroho, A.E. Nugroho, R. Kutsyk, Iraqi Journal of Pharmaceutical Sciences 31 (2022) 150. https://doi.org/10.31351/vol31iss2pp150-159
8. F.O. Abreu, C. Bianchini, T.B. Kist, M.M.C. Forte, Polymer International 58 (2009) 1267. https://doi.org/10.1002/pi.2657

9. D. Maity, A.P. Teixeira, M. Fussenegger, Small 19 (2023) 2301427. https://doi.org/10.1002/smll.202301427
10. C.M. DeRamos, A.E. Irwin, J.L. Nauss, B.E. Stout, Inorganica Chimica Acta 256 (1997) 69. https://doi.org/10.1016/S0020-1693(96)05418-7
11. S. Al-Musa, D. Abu Fara, A.A. Badwan, Journal of Controlled Release 57 (1999) 223. https://doi.org/10.1016/S0168-3659(98)00096-0
12. A.A. Agles, I.C. Bourg, Biomacromolecules 25 (2024) 6403. https://doi.org/10.1021/acs.biomac.4c00447
13. R. Vreeker, L. Li, Y. Fang, I. Appelqvist, E. Mendes, Food Biophysics 3 (2008) 361. https://doi.org/10.1007/s11483-008-9087-2
14. A.R. Cho, Y.G. Chun, B.K. Kim, D.J. Park, Journal of Materials Science 49 (2014) 4612. https://doi.org/10.1007/s10853-014-8163-x
15. S. Asadi, S. Eris, S. Azizian, ACS Omega 3 (2018) 15140. https://doi.org/10.1021/acsomega.8b02498
16. C. Thomas-Busani, J.A. Sarabia-Sainz, J. García-Hernández, T.J. Madera-Santana, L. Vázquez-Moreno, G. Ramos-Clamont Montfort, RSC Advances 10 (2020) 28755. https://doi.org/10.1039/D0RA05135G
17. M. Urbanova, M. Pavelkova, J. Czernek, K. Kubova, J. Vyslouzil, A. Pechova, D. Molinkova, J. Vyslouzil, D. Vetchy, J. Brus, Biomacromolecules 20 (2019) 4158. https://doi.org/10.1021/acs.biomac.9b01052
18. B.E. Larsen, J. Bjørnstad, E.O. Pettersen, H.H. Tønnesen, J.E. Melvik, BMC Biotechnology 15 (2015) 29. https://doi.org/10.1186/s12896-015-0147-7
19. A.A. Syah, A.R. Wijaya, I.A. Malik, D.Y. Siwi, AIMS Environmental Science 12 (2025) 435. https://doi.org/10.3934/environsci.2025020
20. A. Ristić, N. Zabukovec Logar, Nanomaterials 9 (2019) 27. https://doi.org/10.3390/nano9010027
21. R. Sharma, G. Saab, M. Schoukens, T.R.C. Van Assche, J.F.M. Denayer, Applied Materials Today 35 (2023) 101918. https://doi.org/10.1016/j.apmt.2023.101918
22. D. Yu, X. Han, S. Wang, L. Zhong, L. Zhang, M. Zhou, Q. Luo, T. Zhang, L. Zhu, Y. Hou, Y. Zheng, Separation and Purification Technology 331 (2024) 125629. https://doi.org/10.1016/j.seppur.2023.125629
23. F. Luo, X. Liang, W. Chen, S. Wang, X. Gao, Z. Zhang, Y. Fang, Chemical Engineering Journal 465 (2023) 142891. https://doi.org/10.1016/j.cej.2023.142891
24. J. Wang, Y. Dang, A.G. Meguerdichian, S. Dissanayake, T. Kankanam-Kapuge, S. Bamonte, Z.M. Tobin, L.A. Achola, S.L. Suib, Environmental Science & Technology Letters 7 (2020) 48. https://doi.org/10.1021/acs.estlett.9b00713
25. X.Y. Liu, W.W. Wang, S.T. Xie, Q.W. Pan, Scientific Reports 11 (2021) 14412. https://doi.org/10.1038/s41598-021-93784-7
26. R. Li, Y. Shi, M. Alsaedi, M. Wu, L. Shi, P. Wang, Environmental Science & Technology 52 (2018) 11367. https://doi.org/10.1021/acs.est.8b02852
27. F. Ni, N. Qiu, P. Xiao, C. Zhang, Y. Jian, Y. Liang, W. Xie, L. Yan, T. Chen, Angewandte Chemie International Edition 59 (2020) 19237. https://doi.org/10.1002/anie.202007885
28. M. Wu, R. Li, Y. Shi, M. Altunkaya, S. Aleid, C. Zhang, W. Wang, P. Wang, Materials Horizons 8 (2021) 1518. https://doi.org/10.1039/D0MH02051F